Materials Chemistry and Physics 333 (2025) 130327

Contents lists available at ScienceDirect

Materials Chemistry and Physics

journal homepage: www.elsevier.com/locate/matchemphys

Exploring the cytotoxicity and DNA binding studies of green synthesized europium stannate nanoparticle through experimental and computational approach

M.S. Raghu [a], S. Bindu [b], Amar Yasser Jassim [c], K. Yogesh Kumar [d], M.K. Prashanth [e,*], Fahd Alharethy [f], Byong-Hun Jeon [g,**]

[a] Department of Chemistry, New Horizon College of Engineering, Bengaluru, 560 103, India
[b] Department of Electronics & Communication Engineering, B N M Institute of Technology, Bengaluru, 560 070, India
[c] Department of Marine Vertebrate, Marine Science Center, University of Basrah, Basrah, Iraq
[d] Department of Chemistry, Faculty of Engineering and Technology, Jain University, Ramanagara, 562 112, India
[e] Department of Chemistry, B N M Institute of Technology, Bengaluru, 560 070, India
[f] Department of Chemistry, College of Science, King Saud University, Riyadh, 11451, Saudi Arabia
[g] Department of Earth Resources and Environmental Engineering, Hanyang University, 222, Wangsimni-ro, Seongdong-gu, Seoul, 04763, Republic of Korea

HIGHLIGHTS

- The green synthesis of $Eu_2Sn_2O_7$ nanoparticles using pseudo-stem extract of *Musa paradisiaca*.
- The formation of $Eu_2Sn_2O_7$ nanoparticles was confirmed by XRD, SEM, TEM and XPS spectral techniques.
- The $Eu_2Sn_2O_7$ nanoparticles exhibited cytotoxic to A549 and HepG2 cell lines and safety towards normal WI-38 cells.
- The groove binding mode was observed during the interaction of $Eu_2Sn_2O_7$ nanoparticles with ct-DNA using experimental approach.
- The $Eu_2Sn_2O_7$ nanoparticles bind with ct-DNA in good extend and it is supported by molecular docking with 1BNA protein.

GRAPHICAL ABSTRACT

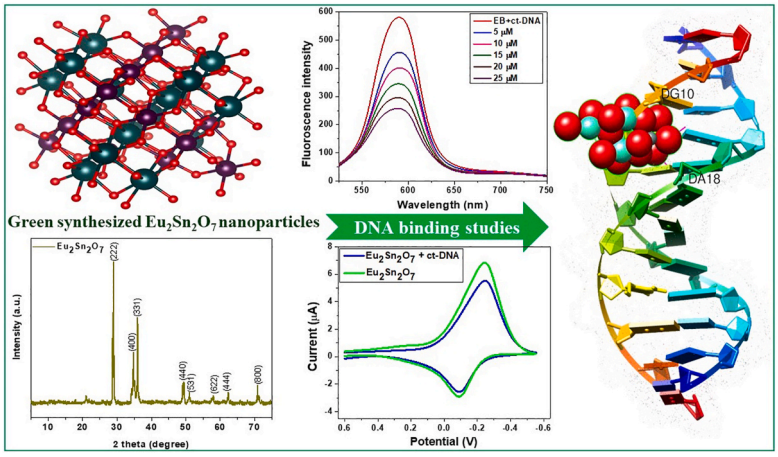

ARTICLE INFO

Keywords:
Europium stannate
Spectroscopy
Cytotoxicity

ABSTRACT

The attention that green synthesized nanoparticles are receiving is owing to their unique biological benefits as well as the physiologically active plant secondary metabolites that support green synthesis. This work reports on the facile, ecofriendly and reliable synthesis of europium stannate ($Eu_2Sn_2O_7$) nanoparticles utilizing pseudo-stem aqueous extract of *Musa paradisiaca*. Pharmacokinetics and pharmacodynamics are greatly impacted by

* Corresponding author.
** Corresponding author.
E-mail addresses: prashanthmk87@gmail.com (M.K. Prashanth), bhjeon@hanyang.ac.kr (B.-H. Jeon).

https://doi.org/10.1016/j.matchemphys.2024.130327
Received 9 September 2024; Received in revised form 11 November 2024; Accepted 22 December 2024
Available online 24 December 2024

DNA binding
Molecular docking

the interactions between drug molecules and DNA as DNA is the primary target of many pharmacological medicines. Therefore, we have investigated the cytotoxic activity and ct-DNA binding of $Eu_2Sn_2O_7$ nanoparticles. Using the MTT test, the cytotoxic potential of $Eu_2Sn_2O_7$ nanoparticles was assessed against A549 and HepG2 cancer cell lines. The results of the cytotoxicity study indicate that the $Eu_2Sn_2O_7$ nanoparticles exhibits improved safety toward normal WI-38 cells and has potential anti-cancer activity, with IC_{50} values of 24.19 and 30.47 μg/mL against the A549 and HepG2 cell lines, respectively. Using circular dichroism, cyclic voltammetry, UV–vis, fluorescence emission spectroscopy, viscosity, and circular dichroism, we have examined the molecular interaction between $Eu_2Sn_2O_7$ nanoparticles and ct-DNA under physiological conditions. This is the first time that a $Eu_2Sn_2O_7$ nanoparticles has been demonstrated to binding with ct-DNA, as far as we are aware. These studies showed that a groove manner of binding between the $Eu_2Sn_2O_7$ nanoparticles and ct-DNA existed. Furthermore, utilizing molecular docking simulations, the binding ability of $Eu_2Sn_2O_7$ nanoparticles with ct-DNA was examined. The outcomes are consistent with the experimental evidence, which shows that hydrogen bonding interactions bind the $Eu_2Sn_2O_7$ nanoparticles to the ct-DNA groove. In a nutshell this information can be utilized to enhance the comprehension of the pharmacological impacts of $Eu_2Sn_2O_7$ nanoparticles in the future.

1. Introduction

Since the beginning of the twentieth century, it has been understood that the sustainability of life and the capacity of a live cell to operate depend greatly on the binding of a drugs to a DNA molecule. The genetic material found in DNA is in charge of several biological functions, including transcription and translation, which are crucial to an organism's ability to grow and develop [1,2]. One crucial area of targeted medicine research is the creation of therapies that specifically target genetic materials like DNA [3]. Because of its potential uses in cytotoxicity and molecular biology research, investigations on the interactions between molecules and DNA have attracted a lot of attention recently [4]. As DNA is the principal target of the majority of anticancer medications, understanding how these drugs interact with DNA may be acquired from studying the binding interactions between DNA and drug molecules. The drug molecules can bind to the sugar phosphate of DNA molecules electrostatically or groove binding, and by intercalation between DNA base pairs [5]. Certain bioactive compounds possessing anticancer characteristics interact through the groove binding mechanism, causing a small disruption in DNA conformations without causing structural distortions [6,7]. Because metal-based chemotherapeutic medicines bind to DNA and block DNA replication, their cytotoxicity is well documented. Therefore, the creation of anticancer metallodrugs depends on the interaction between DNA and nanoparticles, which prompts new studies in pharmacological activities [8,9]. The molecular interaction with ct-DNA is significant in this setting and has been at the centre of cytotoxic activity research.

The crystalline complex materials known as pyrochlores, with the general formula $A_2B_2O_7$, have abundant oxygen sites, variable oxidation states, and versatile structures. Larger rare earth cations, such as Sm, Eu, La, and Ce, often occupy A of the material, whereas smaller transition metals, such as Sn, Ti, and Zr, typically occupy B [10,11]. One such pyrochlore is $Eu_2Sn_2O_7$, which has excellent thermal, optical, and photochemical qualities. As a result, it finds use in optoelectronic devices, batteries, sensors, and photocatalysis applications [12,13]. Due to its variable oxidation state and the continual filling of the 4f orbitals, Eu^{3+} ($4f^7$ $6s^2$) exhibits electrical properties that result in a new band structure. Although $Eu_2Sn_2O_7$ has good optical and luminous properties, its biological uses are yet unknown. Thus, the goal of the current study's authors was to synthesis europium stannate nanoparticles using an environmental benign approach. In India, *M. paradisiaca*, is widely grown and its fruits, peels, and leaves are utilized in a variety of chemical processes [14–16]. It is also frequently known as banana. No pyrochlore-based substance has been synthesized using *M. paradisiaca*'s pseudo-stem as a media. Due to its low cost, less usage of hazardous solvents, good resource efficiency and less toxicity, the green synthesis of $Eu_2Sn_2O_7$ nanoparticles is in great demand.

This work intends to utilize an environmentally friendly method for the synthesis of $Eu_2Sn_2O_7$ nanoparticles as an alternative to traditional techniques, taking into account the great potentiality of plants as sources. To the best of our knowledge, no research on the cytotoxic effects, DNA binding, or green synthesis of $Eu_2Sn_2O_7$ nanoparticles have been reported. Given the above information and keeping with our long-standing interest in creating novel therapeutic agents [17–25], the focus of the current study is on synthesis of $Eu_2Sn_2O_7$ nanoparticles using a pseudo-stem extract from *M. paradisiaca* as reducing agent with their cytotoxic properties' evaluation. Utilizing various spectroscopic methods, the ct-DNA binding experiments of the $Eu_2Sn_2O_7$ pyrochlore have been carried out. In addition, the docking score and hydrogen bonding sites were ascertained utilizing the outcomes of molecular docking.

2. Experimental

2.1. Materials

Precursor materials were obtained from Merck India Pvt, Ltd, Mumbai, India, for the synthesis of nanomaterials. Tris-HCl, EB, and calf thymus DNA (ct-DNA) were acquired from Sigma Aldrich. Without further purification, all of the analytical grade reagents were employed. For studies and reagents preparation, deionized water was utilized.

2.2. Preparation of pseudo-stem extract of M. paradisiaca

We bought the pseudo-stems of *M. paradisiaca* from a local market in Bengaluru. The pseudo-stems were thoroughly washed with running water and allowed to air dry for a day. They were subsequently divided into smaller pieces and extracted using Soxhlet with distilled water for 8 h. The plant extract obtained from the soxhlet extraction process was collected, filtered, and dried for further use.

2.3. Synthesis of europium stannate

A simple and environmentally friendly technique was used to manufacture $Eu_2Sn_2O_7$ nanoparticles utilizing phytochemical extract as a reducing agent. Typically, a 100 mL aqueous solution of tin(IV) chloride pentahydrate and europium(III) nitrate hexahydrate was dissolved in a 1:1 M ratio and agitated continuously for 10 min. About 50 mL of *M. paradisiaca* pseudo-stem extract was gradually added to the solution and sonicated for 10 min. The resultant slurry was transferred to a Teflon-lined autoclave and hydrothermally treated at 120 °C for 4 h. The plant extracts rich in antioxidants, such as flavonoids and polyphenols, to facilitate the reduction of metal ions. This initiated nucleation and subsequent growth of $Eu_2Sn_2O_7$ nanoparticles, with biomolecules from the extract serving to cap and stabilize the nanoparticles, preventing agglomeration [26]. After cooling to ambient temperature, the mixture was filtered and washed three times with ethanol and water. The final product was oven-dried overnight at 80 °C. After drying, the powders were pulverized and kept in airtight containers for later use. The hydrothermal method further enhanced the

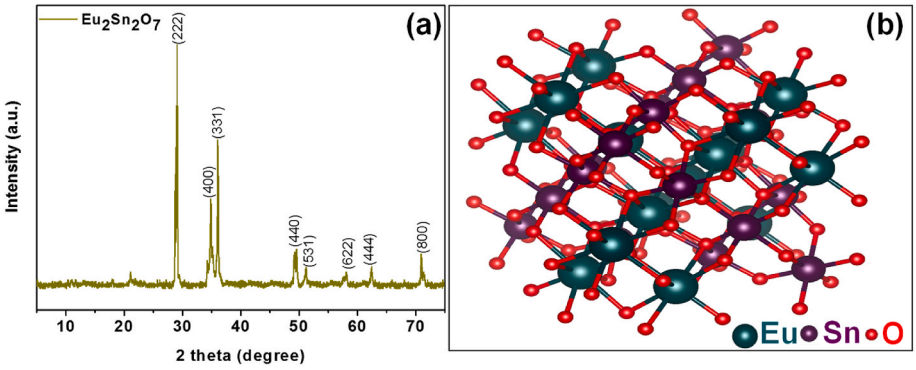

Fig. 1. (a) XRD and (b) crystal structure of $Eu_2Sn_2O_7$.

crystallinity and uniformity of the particles. This combined approach not only minimizes toxic by-products but also improves sustainability and biocompatibility [27].

2.4. Cytotoxicity assay

The cell lines were used in the methylthiazolyl tetrazolium (MTT) test to examine the inhibitory effects of nanoparticles on cell viability. This study uses the human cancer cell lines A549 (lung) and HepG2 (liver), as well as the normal lung fibroblast (WI-38). The assay was carried out following the procedure given in our earlier reported work [28–30]. Nanoparticles concentrations that inhibit cell growth by 50 % (IC_{50}) were estimated using curves produced by plotting cell viability vs nanoparticles concentration.

2.5. Electronic absorption spectra

The absorption spectra were acquired using a Shimadzu UV-2600 spectrophotometer, Japan. In brief, the electronic absorption titration of the $Eu_2Sn_2O_7$ nanoparticles in the aqueous buffer solution (pH 7.4) were done at a constant $Eu_2Sn_2O_7$ nanoparticles concentration (5 μM) and progressively increasing the concentration of ct-DNA (5–30 μM). The baseline was adjusted with Tris-HCl buffer. The intrinsic binding constant (K_b) for $Eu_2Sn_2O_7$ nanoparticles interaction with ct-DNA was estimated by graphing [DNA]/(εa-εf) vs [DNA] using absorption spectral titration data. K_b is calculated using the slope to intercept ratio in this plot.

2.6. Fluorescence spectra

Fluorescence emission tests were performed using a Shimadzu spectrophotometer at room temperature. The fluorescence titration was done by incrementally adding the $Eu_2Sn_2O_7$ nanoparticles (5–25 μM) to the ethidium bromide (EB) pre-treated ct-DNA (10 μM) in Tris-HCl buffer (pH = 7.4) at 25 °C. The fluorescence spectra were obtained at wavelengths ranging from 520 to 750 nm, with an excitation wavelength of 468. The change in fluorescence intensity at 598 nm was recorded, and all measurements were recorded at ambient temperature.

2.7. Circular dichroism studies

CD measurements were made with a rectangular cuvette that had a path length of 1 cm on a Chirascan CD spectropolarimeter. At 25 °C, the CD spectra of ct-DNA (10 μM) were obtained both with (5 and 10 μM) and without $Eu_2Sn_2O_7$ nanoparticles. A 0.5 s time interval and a 1 nm bandwidth were used to record the spectra. After removing the buffer background and averaging four scans, the CD spectrum was obtained.

2.8. Cyclic voltammetry

Using a three-electrode electrochemical setup, the cyclic voltammetric measurements were carried out in the presence and absence of ct-DNA in Tris-HCl buffer (pH 7.4). Ag/AgCl electrode, glassy carbon electrode, and pt-wire serve as the reference, working and auxiliary electrodes in the electrochemical system, respectively. To polish the electrode surface, a Nylon buffer pad containing 0.3 mm of alumina powder was utilized. Prior to the studies, the solution was purged for 1 min with pure nitrogen gas to de-aerate it. A nitrogen stream was then run over the solution to conduct measurements.

2.9. Viscosity measurements

An Ostwald viscometer, kept immersed in a water bath at a consistent 25 °C, was used for the viscosity studies. Viscosities of a 10 μM ct-DNA solution were evaluated both with and without increasing concentrations of the $Eu_2Sn_2O_7$ nanoparticles solution (5–30 μM). Plotting a graph between the relative viscosity and the concentration ratio of $Eu_2Sn_2O_7$ nanoparticles to ct-DNA allowed for the analysis of the data. The sample's viscosity was assessed using the mean of three replicate measurements.

2.10. Molecular docking

The target DNA and $Eu_2Sn_2O_7$ nanoparticles interactions were investigated using AutoDock 4.2 software. The target B-DNA dodecamer protein's crystal structure (PDB ID: 1BNA) was obtained from the Protein Data Bank. The $Eu_2Sn_2O_7$ nanoparticles geometry optimization output file was transformed into a pdb file and used in the docking procedure. After eliminating all ions, water molecules, and any small molecules, polar hydrogen and Gasteiger charges were introduced to the target biomolecule. To fit in to the whole DNA, a grid box of 63 × 63 × 120 with a grid spacing of 0.375 Å was designed. The docking possess was visualized using the Discovery Studio software.

3. Results and discussion

3.1. Structural analysis

To investigate the crystalline structure and phase identification of $Eu_2Sn_2O_7$ nanoparticles, XRD analysis was performed. The resultant $Eu_2Sn_2O_7$ nanoparticles diffraction patterns are shown in Fig. 1a, indicating the successful formation of a high-purity cubic pyrochlore phase with a space group of Fd-3m type. Using the JCPDS: 880457, a brief search showed that all of the diffraction peaks were from the pure crystal phase of $Eu_2Sn_2O_7$ nanoparticles. The diffraction peaks at 29.21°, 34.65°, 36.2°, 49.47°, 51.19°, 58.21°, 62.31°, and 71.02°, respectively match the (222), (400), (331), (440), (531), (622), (444), and (800) hkl

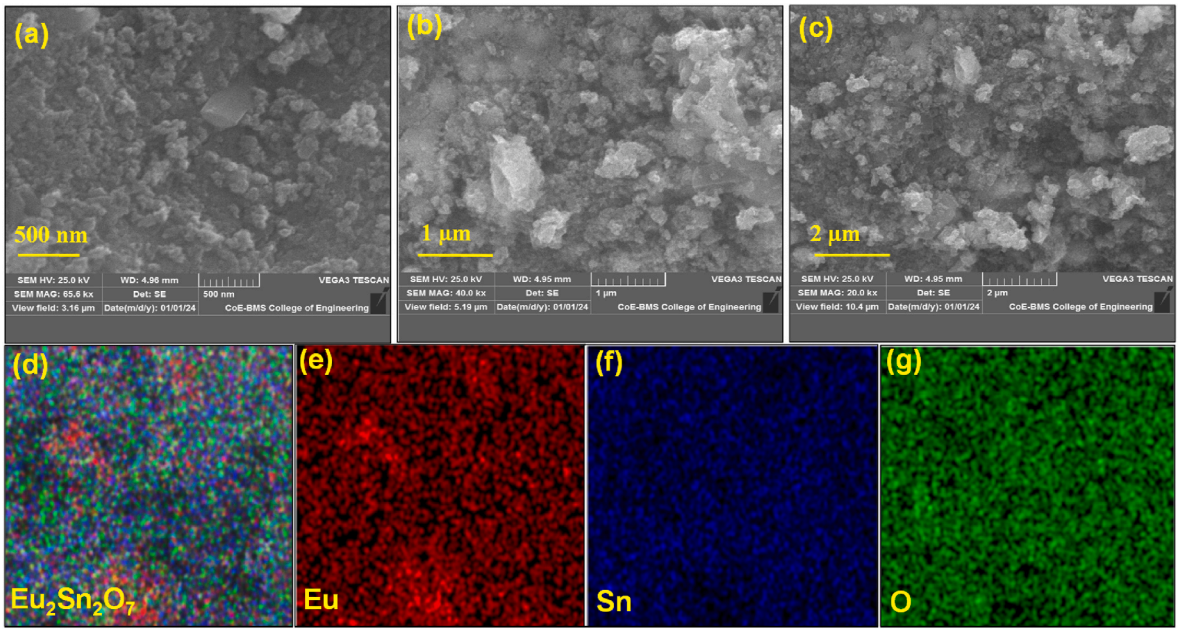

Fig. 2. (a–c) SEM monographs and (d–g) EDS mapping of $Eu_2Sn_2O_7$.

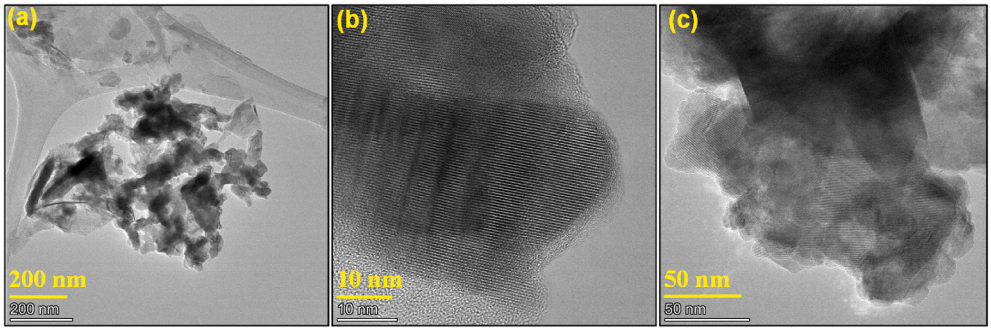

Fig. 3. TEM monographs of $Eu_2Sn_2O_7$.

planes of the cubic lattice [31]. Considering there are no peaks or signs of the development of Eu or Sn hydroxides, this investigation demonstrates the effectiveness of the pseudo-stem extract of *M. paradisiaca* as an effective reducing agent and the obtained particles are in high purity. The intricate crystal structure is seen in Fig. 1b, where the bond between Eu^{3+} and eight O^{2-} atoms acquires a distorted cubic shape centred on the body.

Surface morphology and textural characteristics of $Eu_2Sn_2O_7$ nanoparticles were investigated using TEM and SEM microanalysis. The high-resolution scanning electron micrographs of the unaltered $Eu_2Sn_2O_7$ nanoparticles are shown in Fig. 2a–c. Agglomeration took place during synthesis, as shown in Fig. 2a–c, resulting in the development of a cluster of very small $Eu_2Sn_2O_7$ nanoparticles. However, particles that are between and larger than 100 nm in size show an uneven distribution of their diameters and can form non-homogeneous microstructures. The existence of Eu, Sn, and O in the composites is further confirmed by EDS mapping, and no indications of impurities are seen (Fig. 2d–g). The structure and texture of the $Eu_2Sn_2O_7$ nanoparticles were examined by TEM analysis. The TEM's micrographs (Fig. 3a–c) show the growth of distinct $Eu_2Sn_2O_7$ nanoparticles that range in size from a few nanometres. These little particles form a network of nanoparticles rather than clumping together since they are all interconnected.

The green synthesized $Eu_2Sn_2O_7$ nanoparticles X-ray photoelectron spectroscopy (XPS) investigations are displayed in Fig. 4. The elements Eu 3d, Sn 3d, and O 1s are present in the survey spectrum displayed in Fig. 4a and the other impurities are absent. The two peaks in Fig. 4b, which correspond to the Eu $3d_{5/2}$ and Eu $3d_{3/2}$ subshells, respectively, at 1138.85 and 1166.23 eV, show that europium is in the +3 oxidation state. Sn $3d_{5/2}$ and Sn $3d_{3/2}$ peaks at 490.11 and 499.24 eV, respectively, are assigned to the +4 oxidation state of Sn in the high magnification spectra of Sn 3d shown in Fig. 4c. The presence of lattice oxygen in pyrochlores in Fig. 4d shows two peaks at 531.74 and 533.87 eV, suggesting a better coordination bond between metal and oxygen. These results suggest the synthesis of $Eu_2Sn_2O_7$ nanoparticles of the pyrochlore type.

The N_2 adsorption and desorption isotherms for the $Eu_2Sn_2O_7$ catalysts are depicted in Fig. 5, illustrating the textural characteristics of these materials. The isotherms exhibit type IV behavior, which is typically associated with mesoporous structures. The presence of a pronounced hysteresis loop further confirms this classification, suggesting that the catalysts possess an interconnected network of mesopores with irregular, staggered formations. This structural arrangement facilitates the diffusion of gases through the material, enhancing its adsorption capacity. The specific surface area of $Eu_2Sn_2O_7$ was found to be 68 m^2g^{-1} that increases the cytotoxicity efficiency.

3.2. *Cytotoxic activity*

The A549 and HepG2 cancer cell lines were used to evaluate the *in vitro* cytotoxicity effects of the $Eu_2Sn_2O_7$ nanoparticles. The MTT test

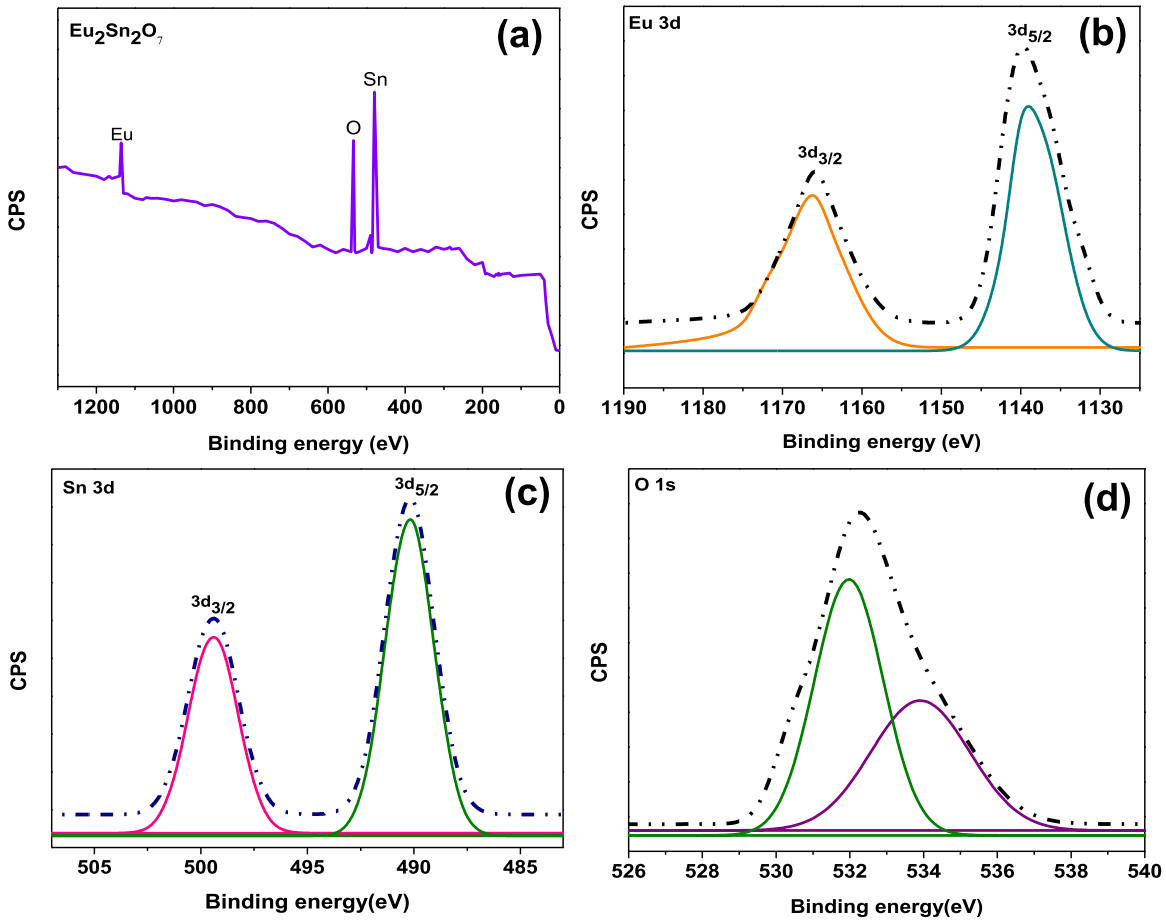

Fig. 4. XPS studies: (a) Survey spectrum, (b) Eu 3d, (c) Sn 3d and (d) O 1s.

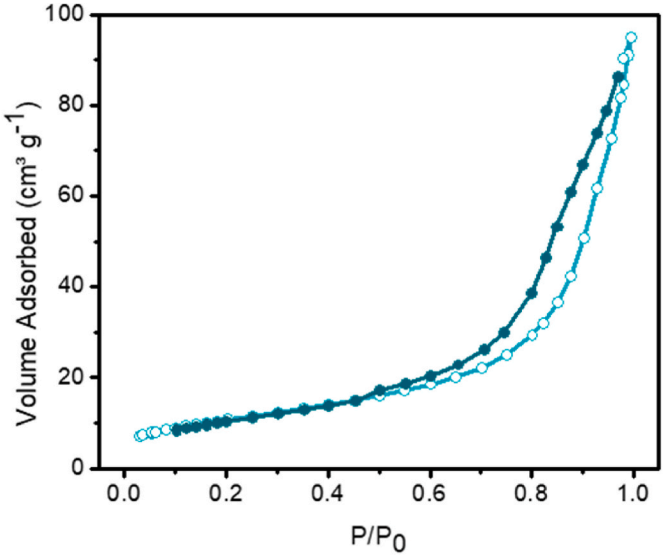

Fig. 5. N_2 adsorption/desorption studies.

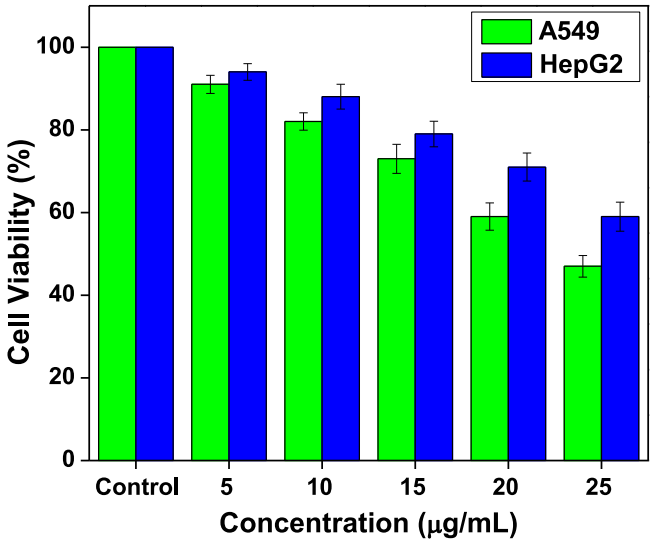

Fig. 6. Cytotoxic effect of $Eu_2Sn_2O_7$ nanoparticles on viability of A549 and HepG2 cell lines.

was used to assess the viability of the cells. The A549 and HepG2 cells' viability was able to be reduced by the $Eu_2Sn_2O_7$ nanoparticles in a dose-dependent way. Fig. 6 displays the $Eu_2Sn_2O_7$ nanoparticles MTT test results on A549 and HepG2 cell lines. After 24 h of incubation with 5–25 μg/mL of $Eu_2Sn_2O_7$ nanoparticles, we found that the growth of cancer cells was supressed by the $Eu_2Sn_2O_7$ nanoparticles, with growth inhibition ranging from 9.36 to 53.28 % in A549 cells and 7.19–41.18 % in HepG2 cells. As compared to the control, the A549 and HepG2 cell lines' cell viability was significantly reduced by the $Eu_2Sn_2O_7$ nanoparticles at a concentration of 25 μg/mL, according to the data displayed in Fig. 6. It is evident that the A549 cell line is more susceptible to the effects of $Eu_2Sn_2O_7$ nanoparticles than the HepG2 cell line. Using non-

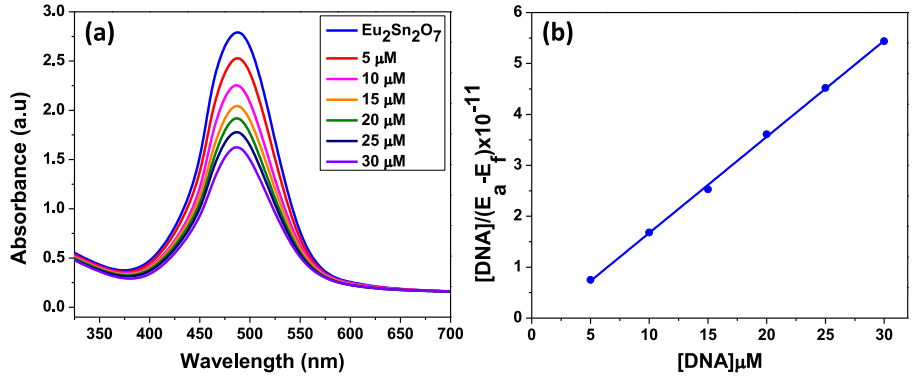

Fig. 7. (a) The absorption spectra of $Eu_2Sn_2O_7$ nanoparticles (5 μM) in absence and presence (5–30 μM) of ct-DNA; (b) Plot of [DNA]/(εa-εf) vs [DNA].

linear regression curves, compound doses that result in 50 % cell growth inhibition (IC_{50}) were determined. For the A549 and HepG2 cell lines, the corresponding r^2 values were 0.9911 and 0.9871. The results showed that the $Eu_2Sn_2O_7$ nanoparticles had IC_{50} values of 24.19 and 30.47 μg/mL against the A549 and HepG2 cell lines, respectively. To ascertain the safety profile of the $Eu_2Sn_2O_7$ nanoparticles, their cytotoxicity impact was assessed against the normal healthy fibroblast cell line, WI-38. The findings demonstrated that the tested $Eu_2Sn_2O_7$ nanoparticles exhibited excellent selectivity profile over tumour cell lines and was non-toxic even at concentrations of 30 μg/mL.

3.3. Electronic spectroscopy

For the evaluation of the interaction between ct-DNA and nanoparticles, electronic absorption spectroscopy is one of the most effective, simplest and straightforward method. Generally, when a molecule interacts with ct-DNA and causes a structural modification in the ct-DNA, changes in absorbance such as hyperchromism and hypochromism are seen. The concentration of ct-DNA is altered in this absorption titration investigation, while the concentration of $Eu_2Sn_2O_7$ nanoparticles is maintained constant. The absorbance titration technique used to track the interaction between a 5 μM $Eu_2Sn_2O_7$ nanoparticles and a 5–30 μM ct-DNA concentration is depicted in Fig. 7a. Absorbance declines without a wavelength red shift when the concentration of ct-DNA in the nanoparticles increases. The observed changes clearly shows that the $Eu_2Sn_2O_7$ nanoparticles is interacted with ct-DNA. On the other hand, no evidence of a wavelength shifts in the direction of longer wavelengths indicated that the $Eu_2Sn_2O_7$ nanoparticles bind to the ct-DNA via groove binding. This shows that the $Eu_2Sn_2O_7$ nanoparticles has great potential for application in developing novel therapeutic agents, as it binds to ct-DNA.

The intrinsic effectiveness of the $Eu_2Sn_2O_7$ nanoparticles with ct-DNA is estimated from the acquired absorption titration data. The value of the binding constant was calculated by plotting [DNA]/(εa-εf) against [DNA] (Fig. 7b). It was observed that the binding constant value was $2.63 \times 10^4\ M^{-1}$. The value of the binding constant measured here is less than that of ethidium bromide, a traditional intercalator, whose binding constant has been reported to be in the range of 10^6-$10^7\ M^{-1}$ [32]. These findings imply a close relationship between the $Eu_2Sn_2O_7$ nanoparticles and ct-DNA, and it's also possible that $Eu_2Sn_2O_7$ nanoparticles bind to the helix through the groove mode [33]. Furthermore, the classical Van't Hoff's equation was utilized to compute the Gibbs free energy (ΔG) of $Eu_2Sn_2O_7$ nanoparticles and ct-DNA, based on the value of the binding constant. The binding of $Eu_2Sn_2O_7$ nanoparticles to ct-DNA was discovered to have a ΔG value of −25.21 kJ/mol. The spontaneous binding of $Eu_2Sn_2O_7$ nanoparticles with ct-DNA was suggested by the negative value of ΔG [34]. The binding constant and Gibbs free energy values of europium stannate nanoparticle with DNA is superior compared to many reported green synthesized materials as depicted in Table 1.

Table 1
Comparison of binding constant and Gibbs free energy values of present work over previously green synthesized nanoparticles with DNA.

SI. No.	Nanoparticle	Binding constant	Gibbs Free energy	Reference
1	Ag NP	$1.18 \times 10^4\ M^{-1}$	−20.87 kJ/mol	[35]
2	Se NP	$2.50 \times 10^3\ M^{-1}$	−13.81 kJ/mol	[36]
3	Ag NP	$6.46 \times 10^3\ M^{-1}$	−22.73 kJ/mol	[37]
4	ZnO NP	$1.55 \times 10^3\ M^{-1}$	not determined	[38]
5	NiO NP	$2.00 \times 10^4\ M^{-1}$	not determined	[39]
6	MnO_2 NP	$1.98 \times 10^4\ M^{-1}$	not determined	[40]
7	Cu NP	$1.02 \times 10^2\ M^{-1}$	not determined	[41]
8	$Eu_2Sn_2O_7$ NP	$2.63 \times 10^4\ M^{-1}$	−25.21 kJ/mol	Present work

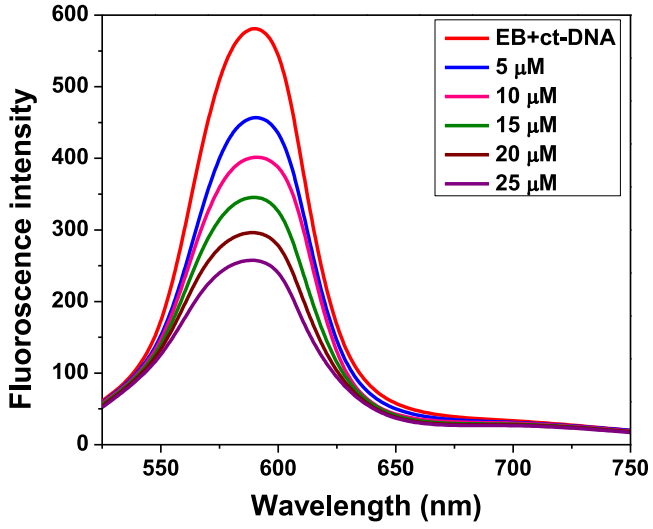

Fig. 8. Emission spectra of EB-ct-DNA in the absence and presence $Eu_2Sn_2O_7$ nanoparticles.

3.4. Fluorescence study

The mechanism of interaction between ct-DNA and $Eu_2Sn_2O_7$ nanoparticles ought to be investigated through the use of fluorescence spectrum analysis. When performing fluorescence quenching experiments using EB-bound ct-DNA and $Eu_2Sn_2O_7$ nanoparticles, these investigations yielded crucial information. By tracking the change in the $Eu_2Sn_2O_7$ nanoparticle's fluorescence intensity, this technique has been frequently utilized to describe the interaction of the nanoparticles with ct-DNA. The observed fluorescence emission spectra of $Eu_2Sn_2O_7$

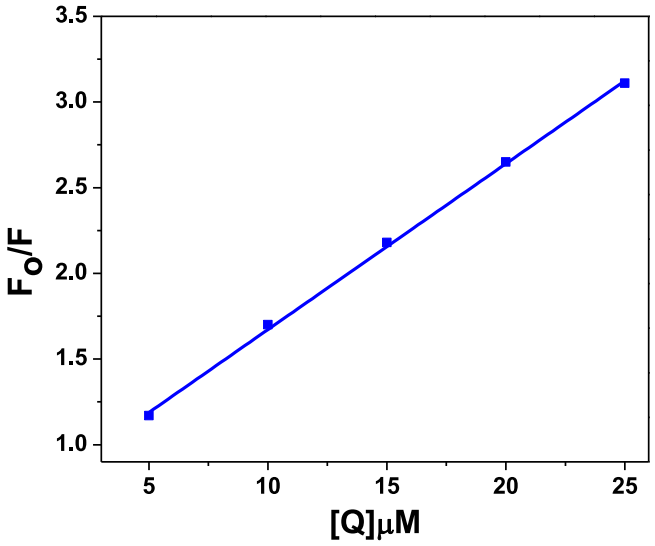

Fig. 9. SV plots for ct-DNA against varying concentration of $Eu_2Sn_2O_7$ nanoparticles.

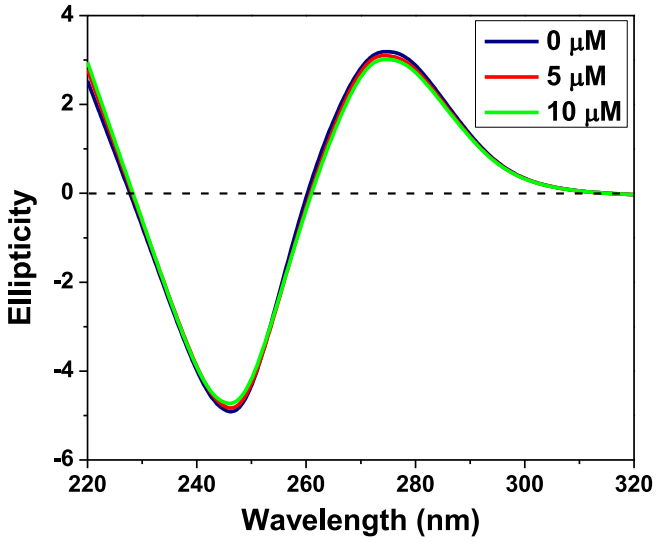

Fig. 10. CD spectra of ct-DNA (10 μM) in the absence and presence of $Eu_2Sn_2O_7$ nanoparticles.

nanoparticles ranged from 5 to 25 μM, whereas the concentration of ct-DNA remained constant at 10 μM. The EB-DNA fluorescent system's observed decrease in intensity with the gradual addition of $Eu_2Sn_2O_7$ nanoparticles at room temperature is depicted in Fig. 7. At 468 nm, the EB-ct-DNA complex was excited, resulting in the observation of its fluorescence emission at 598 nm. As seen in Fig. 8, the fluorescence intensity of the EB-ct-DNA system decreases upon the addition of $Eu_2Sn_2O_7$ nanoparticles to it. The decrease in emission intensity demonstrates that the EB molecules are being quenched as a consequence of the relative binding capability of the $Eu_2Sn_2O_7$ nanoparticles with ct-DNA through the groove binding mode.

The Stern-Volmer equation [42] was used to determine the quenching constant at the quantitative level. The linear Stern-Volmer equation and the fluorescence quenching curve of the EB-ct-DNA system for the $Eu_2Sn_2O_7$ nanoparticles are in good agreement (Fig. 9). The Stern-Volmer quenching constant, which is determined by ratio of the slope to intercept, was found to be 5.81×10^4 M^{-1}. Furthermore, the bimolecular quenching constant, 5.81×10^{12} M^{-1} S^{-1}, may be

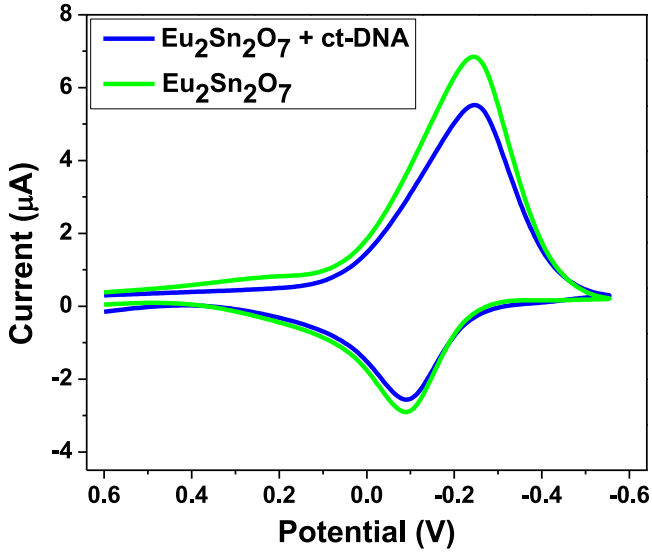

Fig. 11. Cyclic voltammograms of $Eu_2Sn_2O_7$ nanoparticles with and without ct-DNA.

computed. The obtained value is greater than the biomolecule's limiting diffusion rate constant (10^{10} M^{-1} S^{-1}) [43], indicating that the quenching process is static rather than dynamic.

3.5. CD spectral studies

A sensitive and extensively used method for identifying any modification in the DNA backbone during ligand-DNA interactions is CD spectroscopy. Because of base stacking and right-hand helicity, the CD spectra of ct-DNA show a positive band at 275 nm and a negative band at 245 nm, respectively. Fig. 10 displays the results of acquiring CD spectra for ct-DNA (50 μM) at two different concentrations of $Eu_2Sn_2O_7$ nanoparticles. Fig. 10 inferred that a slight decrease in the intensity of both the positive and negative bands was seen with the addition of $Eu_2Sn_2O_7$ nanoparticles. This highlights the possibility of groove binding as a means of ct-DNA and $Eu_2Sn_2O_7$ nanoparticles interaction. The outcome of the CD spectrum analysis shows that there was no conformational change in the DNA secondary structure as a result of the nanoparticles-ct-DNA interaction. Further strong correlations were found between the CD spectral results and the results of absorption and fluorescence spectral studies.

3.6. Cyclic voltammetry study

In recent times, a lot of research has been done on the interaction between molecules and ct-DNA using electrochemical methods, which are simple and rapid to accomplish. It is essential to assess the binding strength and mechanism of drug-DNA interaction under physiological settings using electrochemical techniques like cyclic voltammetry. A glassy carbon electrode was used to record a typical cyclic voltammogram of a 10 μM solution of $Eu_2Sn_2O_7$ nanoparticles without and with ct-DNA (10 μM) in a Tris-HCl buffer (pH 7.4). The anodic and cathodic peak current intensities of the $Eu_2Sn_2O_7$ nanoparticles were both declined when ct-DNA was introduced to the solution. The decline in current might be explained by the $Eu_2Sn_2O_7$ nanoparticle's diffusion after it is bound to the large and slowly diffusing DNA molecule. When a peak potential shifts in a negative direction, it usually means that the molecules are interacting with ct-DNA through groove binding. Both the anodic and cathodic peak potentials showed a minor negative shift, as seen in Fig. 11. These findings imply that groove binding is the mechanism by which $Eu_2Sn_2O_7$ nanoparticles bind with ct-DNA. This cyclic voltammogram results are consistent with the findings from absorption,

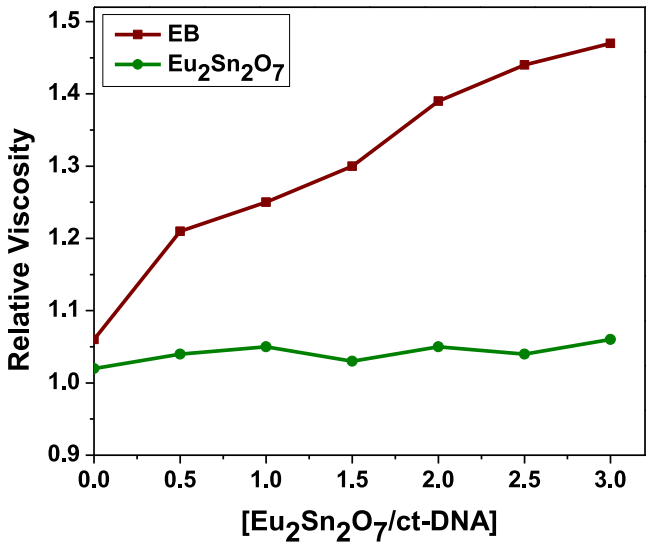

Fig. 12. Effects of increasing amount of EB and $Eu_2Sn_2O_7$ nanoparticles on the relative viscosity of ct-DNA.

fluorescence and CD spectrum investigations mentioned above.

3.7. Viscosity measurements

To back up a binding model, optical photophysical probes give enough information. When testing for a binding in a solution, hydrodynamic measurements like viscosity, which changes as a function of length are considered the most important and least ambiguous. Thus, in order to validate the alteration in the relative viscosities of the ct-DNA, a relative viscosity investigation of the $Eu_2Sn_2O_7$ nanoparticle's ct-DNA interaction studies was carried out using a viscometer. As we know that, when DNA is intercalated in a traditional fashion, the number of base pairs at each site increases, leading to longer DNA and a much thicker DNA solution. Meanwhile, DNA viscosity is almost entirely unaffected by electrostatic and groove binding processes. Fig. 12 displays the results of the viscosity measurements. As an intercalating agent, EB is utilized. The EB causes intercalation by increasing the relative viscosity of DNA. When $Eu_2Sn_2O_7$ nanoparticles are added to ct-DNA solutions, there is no discernible change in the viscosity of the DNA, as seen in Fig. 12. Instead of intercalation, this provided evidence for a groove binding mechanism of $Eu_2Sn_2O_7$ nanoparticles with ct-DNA. Thus, the results of the viscosity measurements corroborate our findings that the $Eu_2Sn_2O_7$ nanoparticles binds to the ct-DNA via the groove binding mechanism, as concluded above by the absorption, fluorescence, CD and CV spectrum data.

3.8. Molecular docking

Molecular docking simulation has surpassed all other methods in computational drug design for estimating ligand-receptor binding affinities [44,45]. The preceding experimental studies demonstrated that $Eu_2Sn_2O_7$ nanoparticles bind to DNA via the groove binding mechanism. We have utilized the molecular docking method to determine the $Eu_2Sn_2O_7$ nanoparticle's interaction with DNA using Autodock software, which supports the experimental findings. DNA is a key therapeutic target for a variety of diseases, including cancer, and it is involved in a wide variety of physiological and biological processes. Anticancer medications have made extensive use of DNA binders in particular. For this reason, DNA is a very attractive target for the creation of medicinal agents [46]. The crystal structure of the protein receptors of the B-DNA dodecamer (PDB ID: 1BNA) was used in this work to perform the molecular docking interaction of $Eu_2Sn_2O_7$ nanoparticles since the crystal structure of ct-DNA was not available in the Protein Data Bank. Fig. 13 displays the $Eu_2Sn_2O_7$ nanoparticle's docking interaction with the target 1BNA protein. According to the docking data, the $Eu_2Sn_2O_7$ nanoparticles fits into a minor groove in DNA that involves contacts without causing any damage to the double helix structure of DNA. With DG10 of the A chain and DA18 of the B chain of DNA, $Eu_2Sn_2O_7$ nanoparticles generate hydrogen bonding interactions with bond distances of 2.43 and 2.39 Å, respectively. The $Eu_2Sn_2O_7$ nanoparticles binding affinity of −7.18 kcal/mol with the 1BNA system suggests that the binding process is spontaneous. We may therefore draw the conclusion that spectroscopic methods and the molecular docked model mutually complement one other, supporting our spectroscopic findings and providing more proof of the groove binding mode.

4. Conclusion

In conclusion, we have successfully employed a hydrothermal technique to green synthesis of $Eu_2Sn_2O_7$ nanoparticles using pseudo-stem extract of *M. paradisiaca*. Using several analytical and physical characterisation techniques, the synthesized $Eu_2Sn_2O_7$ nanoparticles was characterized. $Eu_2Sn_2O_7$ nanoparticles were shown to be more effective against the A549 cell line than the HepG2 cell line in cytotoxicity assays,

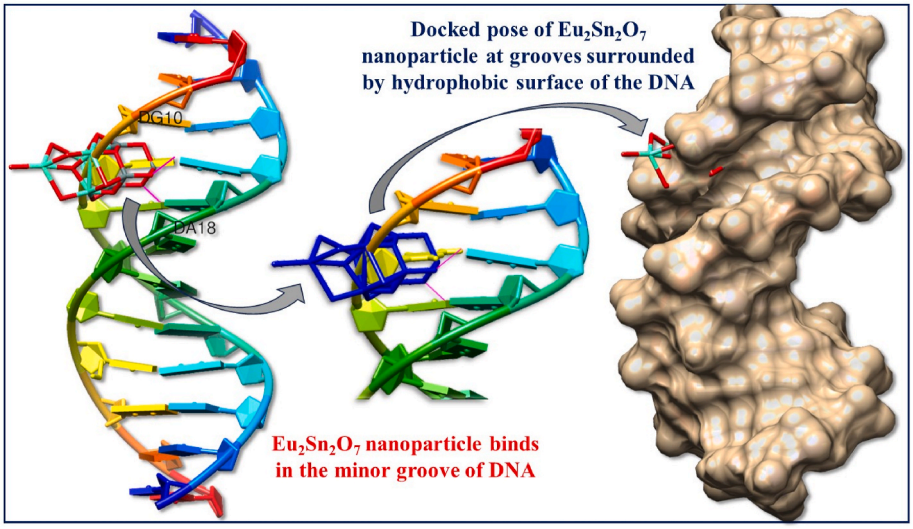

Fig. 13. 3D Docking interaction and surface view of $Eu_2Sn_2O_7$ nanoparticles with target 1BNA protein.

where they inhibited the proliferation of both cell lines in a dose-dependent way. The normal healthy cell line WI-38 is not cytotoxically affected by the $Eu_2Sn_2O_7$ nanoparticles. Various spectral techniques, including electronic absorption, fluorescence, circular dichroism, cyclic voltammetry, and viscometry, were used to investigate the binding efficacy of $Eu_2Sn_2O_7$ nanoparticles with ct-DNT. The results indicate that the binding and Stern-Volmer quenching constants of 2.63 $\times$ 10^4 M^{-1} and 5.81 $\times$ 10^4 M^{-1}, respectively, which suggest a groove mode of binding interactions between the ct-DNA and the $Eu_2Sn_2O_7$ nanoparticles. The spontaneous nature of the binding contact is shown by the Gibbs energy change of −25.21 kJ/mol. Additionally, a molecular docking analysis was carried out to forecast the $Eu_2Sn_2O_7$ nanoparticles binding effectiveness with DNA cavities. The molecular docking studies supported our experimental findings by showing that the minor groove of DNA is bound by the $Eu_2Sn_2O_7$ nanoparticles. Overall, the data show that $Eu_2Sn_2O_7$ nanoparticles have a great deal of promise for use as future agents in DNA binding and chemotherapeutic applications.

CRediT authorship contribution statement

M.S. Raghu: Writing – original draft, Methodology, Investigation. **S. Bindu:** Data curation, Investigation, Methodology. **Amar Yasser Jassim:** Data curation, Formal analysis, Funding acquisition. **K. Yogesh Kumar:** Validation, Investigation, Data curation. **M.K. Prashanth:** Writing – review & editing, Supervision, Methodology, Conceptualization. **Fahd Alharethy:** Visualization, Software, Resources, Data curation. **Byong-Hun Jeon:** Writing – review & editing, Methodology, Conceptualization.

Declaration of competing interest

The authors declare that they have no known competing financial interests or personal relationships that could have appeared to influence the work reported in this paper.

Acknowledgments

The authors immensely express their indebted gratitude to the Management of BNM Institute of Technology for providing lab facilities to carry out this work. The authors extend their thanks and appreciation to Researchers Supporting Project (Ref: RSP2024R160) King Saud University, Riyadh, Saudi Arabia. This work was funded by the Korea Institute of Energy Technology Evaluation and Planning (KETEP) of the Republic of Korea (RS-2023-00255939). Byong-Hun Jeon thank Hanyang University, Seoul, Republic of Korea.

Data availability

No data was used for the research described in the article.

References

[1] S. Minchin, J. Lodge, Understanding biochemistry: structure and function of nucleic acids, Essays Biochem. 63 (2019) 433–456.
[2] O. Humbert, L. Davis, N. Maizels, Targeted gene therapies: tools, applications, optimization, Crit. Rev. Biochem. Mol. Biol. 47 (2012) 264–281.
[3] L. Xuan, Z. Ju, M. Skonieczna, P.K. Zhou, R. Huang, Nanoparticles-induced potential toxicity on human health: applications, toxicity mechanisms, and evaluation models, MedComm 4 (2023) e327.
[4] K. Chen, B.S. Zhao, C. He, Nucleic acid modifications in regulation of gene expression, Cell Chem. Biol. 23 (2016) 74–85.
[5] R. Dinda, S. Majumder, M. Mohanty, D. Mohapatra, S. Aradhana Patra, R. Parida, S. Giri, H. Reuter, C. Kausar, S.K. Patra, Dioxidomolybdenum(VI) complexes of azo-hydrazones: structural investigation, DNA binding and cytotoxicity studies, Polyhedron 227 (2022) 116093.
[6] S. Hussain, S. Shujah, A. Rehman, S.T. Hussain, M. Hussain, I. Naz, A. Alhodaib, Synthesis, spectroscopic characterization, antileishmanial, DNA binding, antioxidant, cytotoxicity, antifungal and antibacterial studies of organotin(IV) carboxylate complexes, Arab. J. Chem. 16 (2023) 105306.
[7] R. Palchaudhuri, P.J. Hergenrother, DNA as a target for anticancer compounds: methods to determine the mode of binding and the mechanism of action, Curr. Opin. Biotechnol. 18 (2007) 497–503.
[8] A.A. Almaqwashi, T. Paramanathan, I. Rouzina, M.C. Williams, Mechanisms of small molecule-DNA interactions probed by single-molecule force spectroscopy, Nucleic Acids Res. 44 (2016) 3971–3988.
[9] R.L. Lucaciu, A.C. Hangan, B. Sevastre, L.S. Oprean, Metallo-drugs in cancer therapy: past, present and future, Molecules 27 (2022) 6485.
[10] K.A. Ajijolakewu, A.S. Ayoola, T.O. Agbabiaka, F.R. Zakariyah, N.R. Ahmed, O. J. Oyedele, A. Sani, A review of the ethnomedicinal, antimicrobial, and phytochemical properties of Musa paradisiaca (plantain), Bull. Natl. Res. Cent. 45 (2021) 86.
[11] R. Sukanya, R. Rajakumaran, S.M. Chen, R. Settu, P. Tharmaraj, Y.R. Lee, Designing of highly active pyrochlore analogous europium stannate electrocatalyst for voltammetric sensing of antibacterial azomycin drug, J. Mol. Liq. 389 (2023) 122919.
[12] S. Gao, R. Wu, M. Sun, M. Guo, D.B. DuBois, S. Chen, H. Ji, C. Wang, Q. Wang, High-performance nitrogen photofixation by Bi2Sn2O7 nanoparticless enriched with oxygen vacancies, Appl. Catal., B 324 (2023) 122260.
[13] V. Jayaraman, A. Mani, Interfacial coupling effect of high surface area Pyrochlore like Ce2Zr2O7 over 2D g-C3N4 sheet photoactive material for efficient removal of organic pollutants, Sep. Purif. Technol. 235 (2020) 116242–116258.
[14] S.M. Abdel Aziz, O.M. Ahmed, S.M. Abd EL-Twab, H.M. Al-Muzafar, K. Adel Amin, M. Abdel-Gabbar, Antihyperglycemic effects and mode of actions of Musa paradisiaca leaf and fruit peel hydroethanolic extracts in nicotinamide/streptozotocin-induced diabetic rats, Evid. Based Complement. Alternat. Med. 2020 (2020) 9276343.
[15] B.O. Ajiboye, H.O. Oloyede, M.O. Salawu, Antihyperglycemic and anti-dyslipidemic activity of Musa paradisiaca-based diet in alloxan-induced diabetic rats, Food Sci. Nutr. 6 (2018) 137–145.
[16] V.D. Kappel, L.H. Cazarolli, D.F. Pereira, B.G. Postal, F.A. Madoglio, Z.S. Buss, F. H. Reginatto, F.R.M.B. Silva, Beneficial effects of banana leaves (Musa x paradisiaca) on glucose homeostasis: multiple sites of action, Rev. Bras. Farmacogn. 23 (2013) 706–715.
[17] C.E. Theodore, G. Sivaiah, S.B. Benaka Prasad, K.Y. Kumar, M.S. Raghu, F. Alharethy, M.K. Prashanth, B.H. Jeon, Design, synthesis, anticancer activity and molecular docking of novel 1H-benzo[d]imidazole derivatives as potential EGFR inhibitors, J. Mol. Struct. 1294 (2023) 136341.
[18] M.S. Raghu, H.A. Swarup, B.S. Prathibha, K. Yogesh Kumar, C.B. Pradeep Kumar, F.A. Alharti, M.K. Prashanth, B.H. Jeon, Design, synthesis and molecular docking studies of 5,6-difluoro-1H-benzo[d]imidazole derivatives as effective binders to GABAA receptor with potent anticonvulsant activity, J. Mol. Struct. 1285 (2023) 135502.
[19] A.G. Alhamzani, T.A. Yousef, M.M. Abou-Krisha, M.S. Raghu, K.Y. Kumar, M. K. Prashanth, B.H. Jeon, Design, synthesis, molecular docking and pharmacological evaluation of novel triazine-based triazole derivatives as potential anticonvulsant agents, Biorg. Med. Chem. Lett. 77 (2022) 129042.
[20] H.N. Deepakumari, B.K. Jayanna, M.K. Prashanth, H.D. Revanasiddappa, B. Veeresh, Synthesis and anticonvulsant activity of N-(substituted)-1-methyl-2,4-dioxo-1,2-dihydroquinazoline-3(4H)-carboxamides, Arch. Pharm. 349 (2016) 566–571.
[21] M. Madaiah, M.K. Prashanth, H.D. Revanasiddappa, B. Veeresh, Synthesis and evaluation of novel imidazo[4,5-c]pyridine derivatives as antimycobacterial agents against Mycobacterium tuberculosis, New J. Chem. 40 (2016) 9194–9204.
[22] M.K. Prashanth, H.D. Revanasiddappa, Synthesis and antioxidant activity of novel quinazolinones functionalized with urea/thiourea/thiazole derivatives as 5-lipoxygenase inhibitors, Lett. Drug Des. Discov. 11 (2014) 712–720.
[23] M. Madaiah, M.K. Prashanth, H.D. Revanasiddappa, B. Veeresh, Synthesis and pharmacological evaluation of novel 1′-[2-(difluoromethoxy) benzyl]-2′ H, 5′ H-spiro [8-azabicyclo [3.2. 1] octane-3, 4′-imidazolidine]-2′,5′-diones and their derivatives, Arch. Pharm. 347 (2014) 370–380.
[24] M. Madaiah, M.K. Prashanth, H.D. Revanasiddappa, Novel synthesis of 4,4difluoropyrido[4,3- b]indoles via intramolecular heck reaction, Tetrahedron Lett. 54 (2013) 1424–1427.
[25] M.K. Prashanth, M. Madaiah, H.D. Revanasiddappa, K.N. Amruthesh, Synthesis, characterization, and BSA binding studies of some new benzamides related to Schiff base, ISRN Org. Chem. 2013 (2013) 1–12.
[26] J.O. Adeyemi, A.O. Oriola, D.C. Onwudiwe, A.O. Oyedeji, Plant extracts mediated metal-based nanoparticles: synthesis and biological applications, Biomol 12 (2022) 627.
[27] M. Yoshimura, K. Byrappa, Hydrothermal processing of materials: past, present and future, J. Mater. Sci. 43 (2008) 2085–2103.
[28] T.A. Yousef, A.G. Alhamzani, M.M. Abou-Krisha, G. Kanthimathi, M.S. Raghu, K. Yogesh Kumar, M.K. Prashanth, B.H. Jeon, Synthesis, molecular docking study and anticancer activity of novel 1, 3, 4-oxadiazole derivatives as potential tubulin inhibitors, Heliyon 9 (2023) e13460.
[29] G. Sivaiah, R. Raveesha, S.B. Benaka Prasad, K.Y. Kumar, M.S. Raghu, F. Alharethy, M.K. Prashanth, B.H. Jeon, Synthesis, anticancer activity and molecular docking of new pyrazolo[1,5-a]pyrimidine derivatives as EGFR/HER2 dual kinase inhibitors, J. Mol. Struct. 1289 (2023) 135877.
[30] G. Sivaiah, M.S. Raghu, S.B. Benaka Prasad, A.M. Anusuya, K. Yogesh Kumar, Fahd Alharethy, M.K. Prashanth, B.H. Jeon, Synthesis, biological evaluation and molecular docking studies of new pyrimidine derivatives as potent dual EGFR/HDAC inhibitors, J. Mol. Struct. 1309 (2024) 138223.

[31] W. Wang, S. Liang, J. Bi, J.C. Yu, P.K. Wong, L. Wu, Lanthanide stannate pyrochlores Ln2Sn2O7 (Ln=Nd, Sm, Eu, Gd, Er, Yb) nanocrystals: synthesis, characterization, and photocatalytic properties, Mater. Res. Bull. 56 (2014) 86–91.
[32] M. Cory, D.D. McKee, J. Kagan, D.W. Henry, J.A. Miller, Design, synthesis, and DNA binding properties of bifunctional intercalators. Comparison of polymethylene and diphenyl ether chains connecting phenanthridine, J. Am. Chem. Soc. 107 (1985) 2528–2536.
[33] Z.H. Xu, F.J. Chen, P.X. Xi, X.H. Liu, Z.Z. Zeng, Synthesis, characterization, and DNA-binding properties of the cobalt(II) and nickel(II) with salicylaldehyde 2-phenylquinoline-4-carboylhydrazone, J. Photochem. Photobiol., A 196 (2008) 77–83.
[34] M.K. Prashanth, K. Chaitra, P. Krishnaiah, K. Prashanth, S. Kumar, F.A. Alharthi, L. Parashuram, M. Raghu, Multifunctional carbon dot anchored halloysite nanotube: nanovehicle for cisplatin drug release, cytotoxicity on breast cancer cells and DNA binding studies, Chemical Data Collections 38 (2022) 100827.
[35] B. Laib, Djahra Ali, O. Boudebia, Green synthesis of silver nanoparticles using Helianthemum lippii extracts (Hl-NPs): characterization, antioxidant and antibacterial activities, and study of interaction with DNA, J. Organomet. Chem. 986 (2023) 122619.
[36] N. Shahabadi, S. Zendehcheshm, F. Khademi, Selenium nanoparticles: synthesis, in-vitro cytotoxicity, antioxidant activity and interaction studies with ct-DNA and HSA, HHb and Cyt c serum proteins, Biotechnol. Rep. 30 (2021) e00615.
[37] S. Roy, R. Sadhukhan, U. Ghosh, T.K. Das, Interaction studies between biosynthesized silver nanoparticle with calf thymus DNA and cytotoxicity of silver nanoparticles, Spectrochim. Acta Mol. Biomol. Spectrosc. 141 (2015) 176–184.
[38] S. Sudha, A. Mary Sara, Green synthesis of ZnONps using Horse gram seed aqueous extract and its in vitro evaluation on antioxidant, antidiabetic, anticancer and DNA binding potential, Mater. Res. Express 10 (2023) 125401.
[39] N. Sarkar, R.S. Sharma, M. Kaushik, Green synthesis and physiochemical characterization of nickel oxide nanoparticles: interaction studies with Calf thymus DNA, Luminescence 35 (2020) 178–186.
[40] P. Karthik, P. Adwin Jose, A. Chellakannu, S. Gurusamy, P. Ananthappan, R. Karuppathevan, V.S. Vasantha, J. Rajesh, S. Ravichandran, M. Sankarganesh, Green synthesis of MnO_2 nanoparticles from *Psidium guajava* leaf extract: morphological characterization, photocatalytic and DNA/BSA interaction studies, Int. J. Biol. Macromol. 258 (2024) 128869.
[41] M.K. Ghosh, S. Sahu, I. Gupta, T.K. Ghorai, Green synthesis of copper nanoparticles from an extract of Jatropha curcas leaves: characterization, optical properties, CT-DNA binding and photocatalytic activity, RSC Adv. 10 (2020) 22027–22035.
[42] M.S. Raghu, K. Yogesh Kumar, K. Veena, C.B. Pradeep Kumar, A.S. Almalki, G. Mani, F.A. Alasmary, M.K. Prashanth, Synthesis, characterization, antimicrobial and interaction studies of pteridines with human serum albumin: a combined multi-spectroscopic and computational study, J. Mol. Struct. 1250 (2022) 131857.
[43] M.K. Prashanth, M.S. Raghu, H.D. Revanasiddappa, B. Veeresh, Synthesis, anticonvulsant and binding interaction study of novel piperamides with bovine serum albumin by fluorescence spectroscopy, Cent. Nerv. Syst. Agents Med. Chem. 16 (2016) 60–66.
[44] M.S. Raghu, C.B. Pradeep Kumar, K.N.N. Prasad, S. Chandrasekhar, K. Yogesh Kumar, M.K. Prashanth, B. Veeresh, MoS 2-calix[4]arene catalyzed synthesis and molecular docking study of 2,4,5-trisubstituted imidazoles as potent inhibitors of Mycobacterium tuberculosis, ACS Comb. Sci. 22 (2020) 509–518.
[45] M.S. Raghu, C.B. Pradeep Kumar, K. Yogesh Kumar, M.K. Prashanth, M. Y. Alshahrani, I. Ahmad, R. Jain, Design, synthesis and molecular docking studies of imidazole and benzimidazole linked ethionamide derivatives as inhibitors of InhA and antituberculosis agents, Bioorg. Med. Chem. Lett. 60 (2022) 128604.
[46] C.B. Pradeep Kumar, M.S. Raghu, K.N.N. Prasad, S. Chandrasekhar, B.K. Jayanna, F.H.A. Alharthi, M.K. Prashanth, K. Yogesh Kumar, Investigation of biological activity of 2,3-disubstituted quinazolin-4(1H)-ones against Mycobacterium tuberculosis and DNA via docking, spectroscopy and DFT studies, New J. Chem. 45 (2021) 403–414.